scientific reports

Check for updates

OPEN

Comparison of the effects of fractional microneedle radiofrequency and microneedling on modulating the senescent fibroblast milieu in aged skin

Jung Min Hwang[1], Soo Hyun Lee[1], Eun Jae Baek[1], Hye-Rin Charlotte Kim[1], Jang-Hee Oh[2,3], Ji Su Lee[2] & Si-Hyung Lee[1,2,3]✉

Skin ageing is a complex and multifaceted biological process that involves the accumulation of senescent dermal fibroblasts. While fractional microneedle radiofrequency (MNRF) is widely used for skin rejuvenation, the underlying molecular mechanisms are unknown. This study aimed to investigate the efficacy of fractional MNRF in altering the cellular milieu of aged skin and to evaluate clinical skin improvements. Thirty female volunteers aged ≥ 60 years with visible periorbital wrinkles received four consecutive treatments of either microneedling or MNRF on randomly assigned facial sides. Based on biophysical measurements, MNRF treatment improved wrinkles, elasticity, hydration, and transepidermal water loss compared to baseline. Histological analysis revealed that the MNRF-treated sides exhibited increased proliferation of non-senescent fibroblasts, a reduced number of senescent fibroblasts, and elevated collagen and elastin levels, compared to the MN-treated sides. In additional analyses, differences in collagen density and hydration between the two sides of the face were statistically significant only in subjects with a marked reduction in senescent fibroblasts in MNRF-treated sides. Our data suggest that, compared to MN, MNRF induces greater clinical and histological improvements in aged skin, likely by altering the dermal fibroblast milieu through the dual effect of eliminating senescent fibroblasts and increasing the number of non-senescent fibroblasts.

Keywords Skin ageing, Cellular senescence, Microneedle radiofrequency, Skin rejuvenation

Skin ageing is a complex, multifaceted biological phenomenon characterised by numerous structural, cellular, and molecular alterations that are driven by intrinsic and extrinsic factors. There are multiple well-known clinical manifestations of skin ageing, such as increased skin laxity, wrinkles, atrophy, roughness, dyschromia and loss of skin volume, elasticity, and hydration[1,2]. Although the intrinsic and extrinsic skin ageing processes are biologically distinct, they mutually influence each other and involve common histological features and functional changes, such as reduced collagen synthesis and increased collagen degradation[3,4].

Cellular senescence, a state of permanent growth arrest and resistance to apoptosis, is a key hallmark of ageing that plays a deleterious role in impeding tissue repair and regeneration, inducing chronic inflammation, and breaking down the extracellular matrix (ECM) via the release of senescence-associated secretory phenotype (SASP) factors[5,6]. Recent studies have shown that ageing phenotypes can be successfully improved in various age-related diseases by removing senescent fibroblasts using senolytic agents[7–9]. Moreover, there have been several reports regarding the elimination of senescent dermal fibroblasts using energy-based systems. Fractional laser resurfacing performed on natural and photoaged skin decreased the levels of DNA damage markers in the dermis and corrected the inappropriate UVB response of epidermal keratinocytes[10]. In addition, the use of fractional microneedle radiofrequency (MNRF) in pulsed wave mode has been shown to be effective in the removal of senescent fibroblasts in melasma and senile lentigo, resulting in a skin-lightening effect[11–14]. However, to date, no study has examined the changes in the composition of senescent and non-senescent fibroblasts and statistically analysed the differences after MNRF application in a sufficiently large cohort of subjects.

[1]Department of Dermatology, Seoul National University College of Medicine, Seoul, Korea. [2]Department of Dermatology, Seoul National University Hospital, Seoul, Korea. [3]Institute of Human-Environmental Interface Biology, Medical Research Centre, Seoul National University, Seoul, Korea. ✉email: shleedm@snu.ac.kr

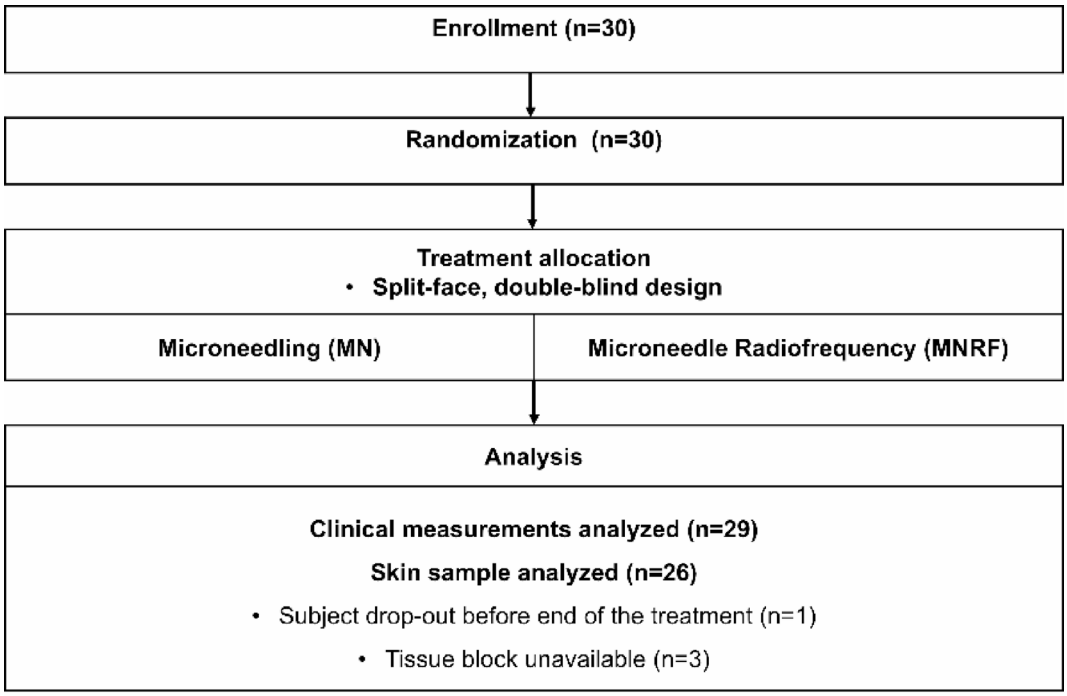

Number of study weeks	0 month (±7days)	1 month (±7days)	2 month (±7days)	3 month (±7days)	5 month (±7days)
Enrollment and training	●				
Biophysical skin measurement	●			●	●
MN/MNRF treatment	●	●	●	●	
Tissue collection					●

Fig. 1. Study flow chart.

Study Subjects, $n = 30$	
Age, years (range)	60–71
(Mean ± SD)	(65.8 ± 2.6)
Gender (n)	
Male	0
Female	30

Table 1. Demographic characteristics of the subjects. n, number of subjects; SD, standard deviation.

Therefore, our study aimed to explore the potency of fractional MNRF in altering the milieu of dermal fibroblasts in aged skin and to evaluate clinical skin improvements. To assess the biological impact of radiofrequency, we compared the performance of microneedling (MN) alone with that of MNRF in a split-face design.

Results

Study population and baseline characteristics

As shown in Fig. 1, 30 subjects were initially recruited for this study. Of these 30 volunteers, 1 individual discontinued participation before the end of the treatment, resulting in a final sample of 29 subjects completing the clinical trial. Histological evaluation was limited to 26 subjects due to specimen loss and technical issues. Table 1 shows the baseline characteristics of the 29 subjects. The study population consisted entirely of Korean women, with a mean age of 65.8 ± 2.6 years (mean ± standard deviation).

Clinical improvements in aged skin after MNRF treatment

Noticeable skin changes from the initial assessment to the 5-month timepoint (2-month follow-up) were found on the MNRF-treated side compared to on the MN-treated side (Fig. 2). The MNRF-treated side showed a progressive improvement in both deep and fine wrinkles. Similar but mild improvements were observed on the MN-treated side.

To evaluate the skin biophysical parameters, statistical analyses were performed to compare baseline values to those observed at the 3- and 5- month timepoints (Table 2). A quantitative measurement of periorbital wrinkles using Visioscan and Visiometer showed improvement over time on both sides, but these advances appeared more quickly and were more profound on the MNRF-treated side. At the 5-month timepoint, both sides showed improvements in the Visioscan measurements. However, at 3 months, a statistically significant difference was seen only in the MNRF-treated side, and the difference at 5 months was even more pronounced on the MNRF-treated side. Consistent with the Visioscan findings, the Visiometer data for the MNRF-treated side showed a noteworthy reduction in skin roughness (R1), maximum roughness (R2), and average roughness (R3) at both 3 and 5 months. A significant decrease was observed in the arithmetic average roughness (R5) at 5 months. However, on the MN-treated side, which showed less improvement compared to the MNRF-treated side, only the maximum roughness (R2) was reduced at both 3 and 5 months, while improvements in skin roughness (R1) and average roughness (R3) were observed exclusively at 5 months.

The assessment of skin elasticity revealed that most indicators that improved were on the MNRF-treated side. The elasticity parameters that improved at both 3 and 5 months on the MNRF-treated side were gross elasticity (R2) and elastic portion (R7). At 5 months, there was a considerable elevation in net elasticity (R5) and significant decline in minimum amplitude (R1) and last minimum amplitude (R4).

In the assessment of skin hydration and TEWL, there was a notable increase in hydration and decrease in TEWL on the MNRF-treated side at 5 months. The melanin and erythema index values showed no statistically significant differences at the two time points compared to at the initial visit on both the MN- and MNRF-treated sides.

Changes in the cellular milieu of the dermis following MNRF treatment

Skin treated with MNRF exhibited an increase in the number of total dermal cells compared to MN-treated skin of the same individual (Fig. 3a). To identify the cell types of the dermal cells that increased in number, we performed immunofluorescence staining for HSP47, a representative fibroblast marker. The subsequent quantification revealed a substantial increase in the number of $HSP47^{+}$ fibroblasts (Fig. 3b). To determine whether inflammatory cells also contributed significantly to the increased dermal cell count, co-staining for CD45, a general leukocyte marker, and CD68, a pan-macrophage marker, was performed. Some skin specimens demonstrated an increase in one or both markers; however, these changes were not statistically significant (Fig. 3c). Therefore, the dermal cells that increased in number after MNRF treatment appeared to be predominantly fibroblasts.

Repopulation of senescent fibroblasts by non-senescent fibroblasts induced by MNRF

To further investigate changes in the characteristics of dermal fibroblasts following MNRF treatment, the senescence marker, $p16^{INK4A}$, was immunolabelled with HSP47 (Fig. 4a). The quantitative assessment revealed not only a significantly lower percentage of $p16^{INK4A}$ expression among $HSP47^{+}$ fibroblasts observed in the MNRF-treated skin (Fig. 4b) but also a reduced absolute number of $p16^{INK4A+}HSP47^{+}$ cells compared to that in the MN-treated skin (Fig. 4c). A similar reduction was observed in the number of dermal $p16^{INK4A+}$ cells in MNRF-treated skin (Fig. 4d). However, on quantifying senescent epidermal cells, the number of $p16^{INK4A+}$ epidermal cells did not differ significantly between MN- and MNRF -treated skin samples (Fig. 4e). As previously noted, there was a marked increase in the number of $HSP47^{+}$ fibroblasts on the MNRF-treated side, and further analysis revealed that most cells did not express p16. This indicated that $p16^{INK4A-}HSP47^{+}$ non-senescent

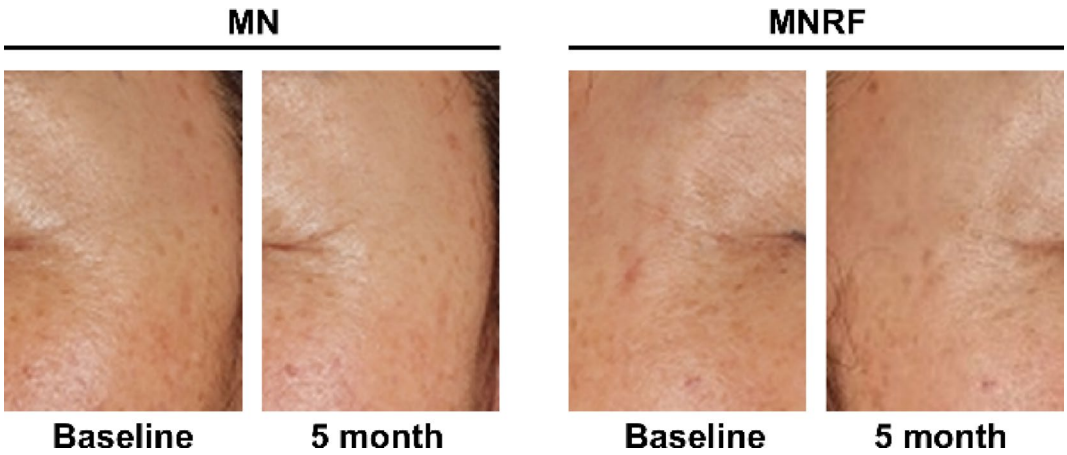

Fig. 2. Split-face comparison in a 69-year-old woman treated with MN or MNRF on each side of the face.

	MN					MNRF				
	Baseline	3 month	Statistical Significance	5 month	Statistical Significance	Baseline	3 month	Statistical Significance	5 month	Statistical Significance
Wrinkles										
Visioscan	98.76 ± 8.26	95.60 ± 10.81	ns($p = 0.284$)	93.35 ± 10.78	**s($p = 0.015$)**	99.01 ± 8.30	93.31 ± 10.96	**s($p = 0.0005$)**	91.11 ± 11.40	**s($p < 0.0001$)**
Visiometer										
R1	1.43 ± 0.29	1.35 ± 0.22	ns($p = 0.073$)	1.23 ± 0.18	**s($p = 0.0004$)**	1.45 ± 0.23	1.31 ± 0.22	**s($p = 0.046$)**	1.19 ± 0.14	**s($p = 0.042$)**
R2	1.11 ± 0.30	1.02 ± 0.20	**s($p = 0.027$)**	0.89 ± 0.18	**s($p = 0.0004$)**	1.07 ± 0.25	0.92 ± 0.21	**s($p = 0.003$)**	0.85 ± 0.16	**s($p = 0.0001$)**
R3	0.66 ± 0.17	0.63 ± 0.11	ns($p = 0.242$)	0.58 ± 0.10	**s($p = 0.008$)**	0.64 ± 0.13	0.58 ± 0.11	**s($p = 0.024$)**	0.55 ± 0.09	**s($p = 0.021$)**
R4	0.45 ± 0.07	0.45 ± 0.07	ns($p = 1.000$)	0.45 ± 0.06	ns($p = 1.000$)	0.45 ± 0.06	0.43 ± 0.07	ns($p = 0.681$)	0.43 ± 0.08	ns($p = 0.743$)
R5	0.20 ± 0.04	0.20 ± 0.05	ns($p = 1.000$)	0.20 ± 0.04	ns($p = 1.000$)	0.22 ± 0.05	0.21 ± 0.05	ns($p = 0.429$)	0.18 ± 0.03	**s($p = 0.005$)**
Elasticity										
R0	0.25 ± 0.06	0.24 ± 0.06	ns($p = 0.920$)	0.22 ± 0.07	ns($p = 0.130$)	0.25 ± 0.06	0.25 ± 0.06	ns($p = 0.982$)	0.22 ± 0.06	ns($p = 0.125$)
R1	0.10 ± 0.04	0.10 ± 0.04	ns($p = 1.000$)	0.09 ± 0.04	ns($p = 0.150$)	0.11 ± 0.03	0.10 ± 0.03	ns($p = 0.445$)	0.09 ± 0.03	**s($p = 0.005$)**
R2	0.60 ± 0.08	0.58 ± 0.07	ns($p = 0.482$)	0.61 ± 0.08	ns($p = 1.000$)	0.56 ± 0.07	0.60 ± 0.07	**s($p = 0.013$)**	0.62 ± 0.07	**s($p = 0.0001$)**
R3	0.28 ± 0.06	0.27 ± 0.07	ns($p = 1.000$)	0.25 ± 0.08	ns($p = 0.109$)	0.28 ± 0.07	0.28 ± 0.06	ns($p = 0.795$)	0.26 ± 0.07	ns($p = 0.112$)
R4	0.14 ± 0.05	0.14 ± 0.05	ns($p = 1.000$)	0.12 ± 0.05	**s($p = 0.024$)**	0.15 ± 0.04	0.13 ± 0.04	ns($p = 0.451$)	0.12 ± 0.04	**s($p = 0.007$)**
R5	0.48 ± 0.14	0.46 ± 0.11	ns($p = 0.163$)	0.50 ± 0.14	ns($p = 0.829$)	0.45 ± 0.14	0.48 ± 0.11	ns($p = 0.177$)	0.52 ± 0.13	**s($p = 0.005$)**
R6	0.68 ± 0.19	0.69 ± 0.19	ns($p = 1.000$)	0.69 ± 0.18	ns($p = 1.000$)	0.68 ± 0.19	0.66 ± 0.16	ns($p = 1.000$)	0.71 ± 0.18	ns($p = 1.000$)
R7	0.28 ± 0.06	0.27 ± 0.05	ns($p = 0.809$)	0.29 ± 0.06	ns($p = 1.000$)	0.27 ± 0.05	0.29 ± 0.05	**s($p = 0.040$)**	0.30 ± 0.05	**s($p = 0.002$)**
R8	0.15 ± 0.03	0.14 ± 0.03	ns($p = 0.249$)	0.13 ± 0.04	ns($p = 0.103$)	0.14 ± 0.04	0.15 ± 0.03	ns($p = 0.094$)	0.14 ± 0.04	ns($p = 0.459$)
R9	0.03 ± 0.01	0.03 ± 0.01	ns($p = 1.000$)	0.03 ± 0.01	ns($p = 0.276$)	0.03 ± 0.01	0.03 ± 0.01	ns($p = 1.000$)	0.03 ± 0.01	ns($p = 1.000$)
Hydration	59.28 ± 7.49	61.71 ± 8.91	ns($p = 0.1000$)	61.71 ± 10.50	ns($p = 0.635$)	59.61 ± 8.05	64.04 ± 8.69	ns($p = 0.081$)	64.27 ± 9.10	**s($p = 0.016$)**
TEWL	11.23 ± 2.60	10.42 ± 2.52	ns($p = 0.347$)	10.11 ± 2.84	ns($p = 0.091$)	11.35 ± 2.86	10.49 ± 2.34	ns($p = 0.338$)	10.03 ± 2.10	**s($p = 0.046$)**
Melanin Index	163.30 ± 43.85	168.71 ± 39.59	ns($p = 0.069$)	173.24 ± 33.54	ns($p = 0.056$)	161.25 ± 39.29	165.53 ± 39.12	ns($p = 0.945$)	169.45 ± 33.78	ns($p = 0.327$)
Erythema Index	227.96 ± 76.42	223.90 ± 74.40	ns($p = 0.762$)	217.55 ± 78.74	ns($p = 0.449$)	230.78 ± 59.00	230.69 ± 69.51	ns($p = 0.538$)	227.12 ± 66.87	ns($p = 0.538$)

Table 2. Changes in wrinkles, elasticity, hydration, TEWL, melanin index and erythema index induced by treatment with MN or MNRF. Mean ± SD. In bold, statistically significant differences with baseline. Skin wrinkling parameters measured by Visiometer: R1, Skin roughness; R2, Maximum roughness; R3, Average roughness; R4, Smoothness depth; R5, Arithmetic average roughness. Skin elasticity parameters measured by Cutometer: R0, Maximum amplitude; R1, Minimum amplitude; R2, Gross elasticity; R3, Last maximum amplitude; R4, Last minimum amplitude; R5, Net elasticity; R6, Portion of viscoelasticity; R7, Elastic portion; R8, Complete relaxation (R0-R1); R9, Tiring effect (R3-R0). ns, not statistically significant; s, statistically significant; SD, standard deviation; MN, microneedling; MNRF, microneedle radiofrequency; TEWL, trans epidermal water loss.

fibroblasts significantly increased after MNRF treatment (Fig. 4f). Taken together, in response to MNRF, the proportion of senescent fibroblasts decreased, while being simultaneously replenished and exceeded by non-senescent, freshly proliferated fibroblasts.

Improvements in the skin ageing phenotype promoted by MNRF treatment and its association with senescent fibroblasts

Procollagen-1 was immunostained to determine whether de novo collagen synthesis in dermal fibroblasts was activated in MNRF-treated skin, and a notable increase in the number of procollagen-1^{+} cells was observed compared to that in MN-treated skin (Fig. 5a). Quantitative analysis of dermal collagen deposition (Fig. 5b) and elastin fluorescence intensity (Fig. 5c) also revealed a marked increase in the papillary dermis of MNRF-treated skin. Neither collagen deposition nor elastic fibre density in the reticular dermis differed significantly between the two facial sides. These findings suggested that MNRF primarily affects the papillary dermis by stimulating neocollagenesis and neoelastogenesis.

Remarkable epidermal changes were also observed on measuring the epidermal thickness (Supplementary Fig. S1a) and performing immunofluorescence staining for the proliferation marker, ki-67 (Supplementary Fig. S1b). Quantitative results indicated that MNRF induced an increase in the number of proliferating epidermal cells, contributing to the thickening of the epidermis.

To investigate whether MNRF-induced skin changes are associated with alterations in the senescent fibroblast milieu, we divided the subjects into two groups based on the difference in the number of p16$^{INK4\ A+}$HSP47^{+} senescent fibroblasts between the two facial sides. The first group, MNRF-responders, included individuals in the upper 50% of the delta value, demonstrating a significantly decreased number of p16$^{INK4\ A+}$HSP47^{+} cells/mm^2 on the MNRF-treated side compared to MN-treated side (mean ± SD of MNΔMNRF; 147.0 ± 51.3). The second group, MNRF-non-responders, comprised subjects in the lower 50%, showing a minimal reduction or an increase in the number of p16$^{INK4\ A+}$HSP47^{+} cells/mm^2 on the MNRF-treated side compared to MN-treated side (mean ± SD of MNΔMNRF; 4.1 ± 33.0). Through subgroup analysis, we compared the differences in skin

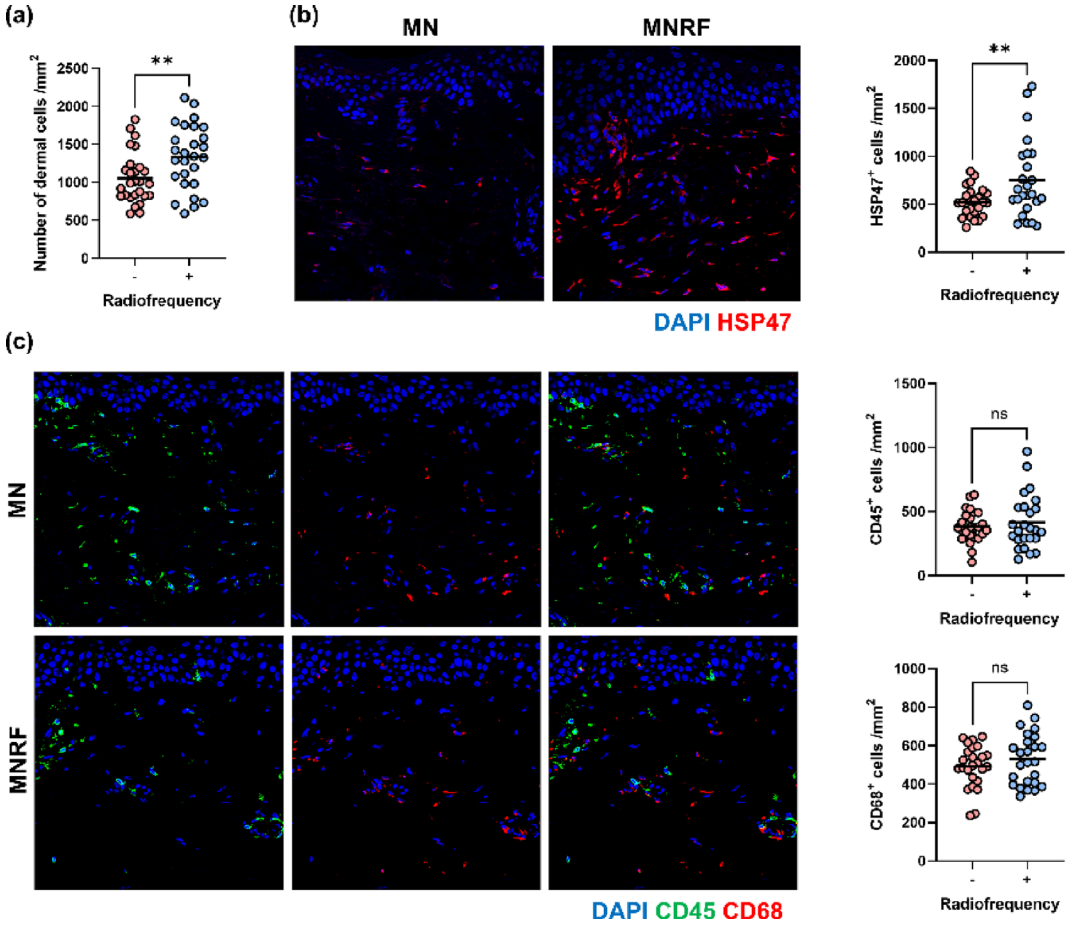

Fig. 3. Changes in the cellular milieu in the dermis following MNRF treatment. (a) Quantification of the total cell number in the dermis after MN and MNRF treatments. (b) Representative images of immunofluorescence staining for the fibroblast marker, HSP47 (red), and DAPI (blue) in the skin treated with MN and MNRF. The graph on the right indicates the number of HSP47-positive dermal fibroblasts after MN and MNRF treatments ($n = 25$). (c) Representative images of immunofluorescence staining for the leukocyte marker, CD45 (green); and macrophage marker, CD68 (red); and DAPI (blue) in skin treated with MN and MNRF. The graphs on the right represent the number of CD45-positive leukocytes and CD68-positive macrophages in the dermis after MN and MNRF treatments ($n = 25$). Original magnification ×400. Statistical significance: $^{**}p < 0.01$, ns indicates no significance.

ageing-related indicators between the two sides of the face in responders, who exhibited pronounced differences in senescent fibroblasts, and in non-responders, who did not. Collagen density and hydration showed significant differences between the two sides only in the responders (Fig. 5d). This indicated that the reduction in senescent fibroblasts was closely associated with collagen density and hydration.

Comparison of adverse skin effects after MN and MNRF treatments

Treatment-related side effects were evaluated by the subjects and dermatologists before and after the treatment sessions. The adverse reactions are shown in Table 3. Although some side effects were experienced more often on the MNRF-treated side, no significant differences in the frequencies of developing immediate erythema, oedema, bruising, pruritus, or a tingling sensation were observed between the two sides ($p > 0.05$). The reported adverse reactions were graded as mild in intensity and well tolerated by all subjects. The durations of adverse events were comparable between the MN and MNRF treatments, ranging from 10 min to 7 days. These skin reactions were mostly managed well by cold compression.

Discussion

Fractional MNRF is a minimally invasive, non-ablative procedure performed with a device that employs a standard microneedle therapy system (MTS) to transmit RF energy directly to desired skin depths using microneedles[15]. In recent years, considerable attention has been focused on fractional MNRF as a method for skin rejuvenation. Although numerous studies on MNRF have examined its efficacy for tightening the skin and diminishing facial rhytids[16–18], there is limited research exploring the underlying cellular and molecular processes that lead to the observed enhancement in clinical appearance.

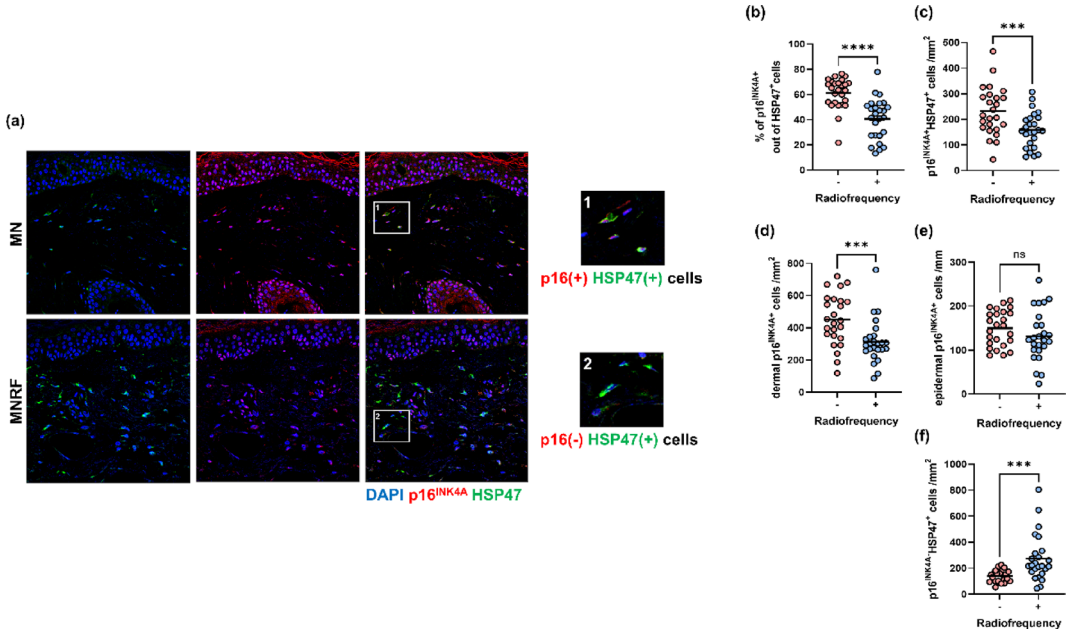

Fig. 4. Repopulation of senescent fibroblasts by non-senescent fibroblasts after MNRF treatment. (a) Representative images of immunofluorescence staining for the senescence marker, $p16^{INK4A}$, and fibroblast marker, HSP47, after MN and MNRF treatments. The graphs on the right represent the results of the quantitative assessment of the (b) percentage of $p16^{INK4A}$-positive cells among HSP47-positive dermal fibroblasts, (c) number of $p16^{INK4A}$- and HSP47- double positive dermal fibroblasts, (d) $p16^{INK4A}$-positive dermal cells, (e) $p16^{INK4A}$-positive epidermal cells, and (f) $p16^{INK4A}$-negative HSP47-positive dermal fibroblasts in the skin treated with MN and MNRF ($n = 25$). Original magnification ×400. Statistical significance: $^{***}p < 0.001$, $^{****}p < 0.0001$. ns indicates no significance.

When MNRF is applied, the resulting thermal damage triggers an active wound healing response and initiates a cascade of growth factors, leading to the de novo synthesis of collagen, elastin, and hyaluronic acid[19,20]. Previous reports have indicated that complete healing after MNRF occurs within a timeframe ranging from 2 to 10 weeks[21–23]. In this study, we obtained tissue samples 8 weeks after the final treatment session to investigate the changes in the cellular milieu of the dermis. Our findings revealed no statistically significant differences in the presence of inflammatory cells, including leukocytes and macrophages, between the facial sides treated with MN and MNRF. Additionally, the observed increase in procollagen-1, collagen, and elastin levels in the papillary dermis and thickening of the epidermis indicated that the wound healing process had been completed, and subsequent skin rejuvenation was successfully initiated.

As ageing progresses, the overall quantity of dermal fibroblasts decreases, whereas the proportion of senescent fibroblasts increases[24,25]. In the present study, we demonstrated that MNRF treatment significantly lowered the count of $p16^{INK4\ A+}$ senescent fibroblasts in aged skin, compared to MN. Since a previous study demonstrated the presence of cleaved caspase-3- and TUNEL-positive cells 3 days after MNRF treatment, RF thermal energy-induced apoptosis has been proposed as an explanation for the reduction in senescent fibroblasts following MNRF application[13] The reduction in the number of senescent dermal fibroblasts would lead to a decline in the release of SASP factors[7,26]. This would eventually diminish chronic inflammation and reduce the levels of proteolytic enzymes, thereby halting ECM breakdown[24]. Concurrent with the reduction in the number of senescent fibroblasts, a significant increase in non-senescent fibroblasts occurred during the wound healing process, leading to enhanced collagen and elastin production. Further analysis revealed that greater improvement in collagen density and hydration was observed in individuals with more pronounced changes in the composition of senescent fibroblasts after MNRF application, implying that the reduction in senescent fibroblasts is not merely a phenomenon induced by MNRF but also a mechanism that improves skin ageing. We propose that the underlying process of MNRF in modulating the fibroblast milieu is that RF thermal energy induces non-specific apoptosis of dermal fibroblasts (both senescent and non-senescent), followed by the proliferation of regenerated non-senescent fibroblasts, ultimately leading to de novo synthesis of collagen and elastin. However, this hypothesis needs to be validated by additional experimentation.

In addition to histological investigations, skin rejuvenation was clinically assessed using biophysical measurements. While both treatments showed improvements over time, MNRF induced earlier and more pronounced effects in most parameters including wrinkles, elasticity, hydration, and TEWL. Microneedling also yielded some improvement, particularly in wrinkle reduction, though to a lesser extent. Notably, the improvements in hydration and TEWL metrics observed with MNRF suggest a potential enhancement in barrier function. Moreover, no significant changes in the melanin and erythema index on either side of the face represent a minimal risk of post-inflammatory hyperpigmentation.

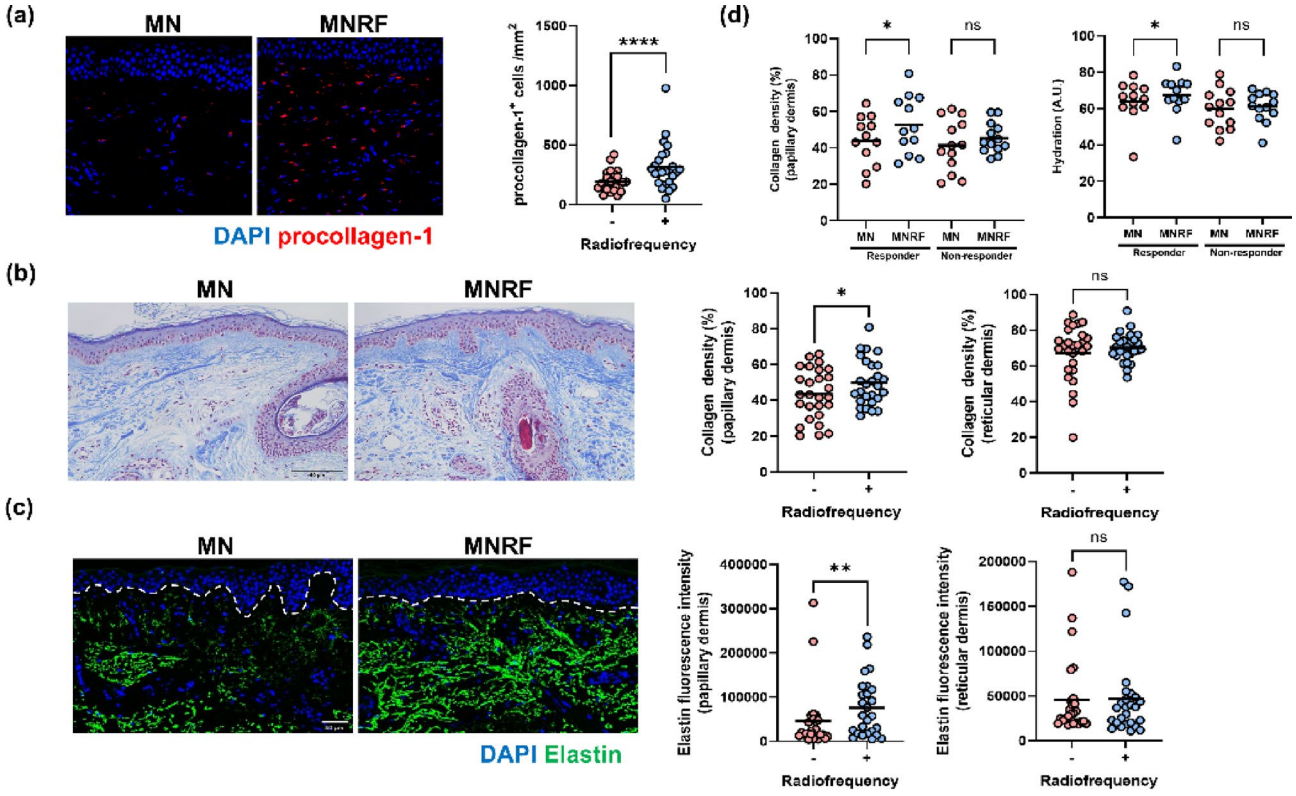

Fig. 5. Improvements in the skin ageing phenotype promoted by MNRF treatment and its association with senescent fibroblasts. (a) Representative images of immunofluorescence staining for procollagen-1 (red) and DAPI (blue) after MN and MNRF treatments. The graph on the right indicates the number of procollagen-1-positive cells after MN and MNRF treatments ($n = 25$). Original magnification ×400. (b) Representative images of dermal collagen deposition using Masson's trichrome staining in the skin treated with MN and MNRF. The graphs on the right represent the results of the quantitative assessment of dermal collagen density in the papillary and reticular dermis after MN and MNRF treatments ($n = 26$). Scale bar = 50 µm. (c) Representative images of immunofluorescence staining for elastin (green) and DAPI (blue) after MN and MNRF treatments. The graphs on the right represent the results of the quantitative assessment of dermal elastic fibres in the papillary and reticular dermis after MN and MNRF treatments ($n = 25$). Scale bar = 50 µm. (d) The graphs indicate the evaluation of collagen density of papillary dermis (left) and hydration (right) in the skin treated with MN and MNRF of MNRF- responders ($n = 12$) and non-responders ($n = 13$). MNRF- responders and non-responders were distinguished based on differences in the number of senescent fibroblasts. Statistical significance: $^{*}p < 0.05$, $^{**}p < 0.01$, $^{****}p < 0.0001$. ns indicates no significance.

Adverse reactions	No. of affected subjects/ total No. of patients (%)		
	MN	MNRF	Statistical Significance
Immediate erythema	0/29 (0.00)	4/29 (13.79)	ns($p = 0.056$)
Edema	0/29 (0.00)	2/29 (6.90)	ns($p = 0.246$)
Bruise	1/29 (3.45)	1/29 (3.45)	ns($p = 0.754$)
Pruritus	1/29 (3.45)	1/29 (3.45)	ns($p = 0.754$)
Tingling sensation	0/29 (0.00)	1/29 (3.45)	ns($p = 0.500$)

Table 3. Adverse reactions after treatment with MN and MNRF. ns, not statistically significant; MN, microneedling; MNRF, microneedle radiofrequency.

In our study, we evaluated the skin-rejuvenating capabilities of MNRF in comparison with those of MN alone. Various intrinsic factors, including variations in wound-healing capacity, skin ageing, and skin barrier function, as well as extrinsic factors such as UV exposure and personal lifestyle, are likely to influence individual responses to MN and MNRF treatments. To mitigate the potential impact of these confounding variables, we conducted a split-face comparison with a large study group and applied paired statistical tests to assess the effects of MN and MNRF within each individual. Although MN by itself is a well-known anti-ageing treatment for facial

rhytides[27,28], MNRF treatment surpassed the extent of MN alone, producing notable improvements in both clinical and histological aspects. To the best of our knowledge, this study is the first prospective investigation with a considerable number of participants to demonstrate and report alterations in the phenotype of skin ageing resulting from senescent cell elimination and subsequent replacement by newly generated fibroblasts after MNRF application.

However, our study has some limitations. First, we lacked pre-treatment skin tissue samples from each subject, preventing us from evaluating changes in the tissue from the initial to post-treatment state. In addition, we could not evaluate long-term effects after MNRF treatment because we completed clinical measurements and obtained tissue 2 months after the last treatment. While other studies have reported that treatment effects persist for 6 months following a single session[29,30], we are unable to address concerns regarding the longevity of these skin enhancements, their long-term safety, or their potential impact on future skin ageing processes. Future research should consider conducting extended trials to examine the long-term effects of MNRF.

In summary, our study compared the performance of MN and MNRF treatments on aged skin, providing a comprehensive understanding of their differential effects on skin rejuvenation at the cellular, histological, and clinical levels. In particular, our results suggest that, compared to MN, MNRF more effectively promotes skin rejuvenation by facilitating senescent cell removal and stimulating the proliferation of non-senescent cells -mechanisms likely underlying its superior histological and clinical outcomes. These findings indicate its potential in the treatment of skin conditions associated with increased senescent fibroblasts, such as melasma and idiopathic guttate hypomelanosis, and are expected to contribute to the ongoing development and advancement of energy-based methodologies for skin rejuvenation, ultimately combating skin ageing.

Materials and methods

Study design

A 5-month-prospective, double-blind, spilt-face, randomised controlled clinical trial was conducted at the Department of Dermatology of Seoul National University Hospital (Seoul, Korea) between February 2022 and March 2024. The study was conducted in accordance with the Declaration of Helsinki and was approved by the Institutional Review Board of Seoul National University Hospital (No. 2101-109-1190). Thirty volunteers aged ≥ 60 years with visible fine wrinkles in the periorbital area were enrolled after providing written informed consent. The bilateral periorbital areas of each subject were randomly assigned to receive either MNRF or MN treatment, and the study was conducted with both the subjects and evaluators blinded to the assignments. A computer-based random number allocator was used for the randomisation. The subjects then underwent 4 sequential sessions of either MN or MNRF treatment on a random side of their face. The treatment procedure involved 4 sequential sessions conducted at 4-week intervals, followed by a final assessment 8 weeks after the final treatment. During each visit, standardised digital photographs were obtained using consistent camera settings (EOS90D; Canon, Tokyo, Japan) and illumination conditions.

MN and MNRF treatments

According to the randomisation table, half the face of each subject was treated with MN and the other half with MNRF (Sylfirm X; Viol Co., Ltd., Seongnam, Korea). The treatment was applied to a consistent area between the lateral canthus and hairline, extending from the eyebrow above to the zygomatic area below. On the MNRF treatment side, the continuous mode (CW4, 300 ms exposure) was used with a 1-mm microneedle depth and energy levels ranging from 3 to 5 (2.42–2.74 J/shot) for one pass, while on the MN side, only microneedling was performed at the same depth with an energy level of 0. After the procedure, the subjects were monitored for 30 min to check for potential adverse skin reactions in the treatment area.

Measurements of biophysical characteristics of the skin

Biophysical skin parameters, including wrinkles, elasticity, hydration, transepidermal water loss (TEWL), melanin index, and erythema index, were measured at baseline and at 3 and 5 months. All clinical skin measurements were performed by a single investigator to ensure data consistency. Each parameter was measured in triplicate in the same fixed periorbital area, and the mean values were used for subsequent analyses. Further information regarding the instruments used for the measurements is provided in Supplementary Materials and Methods section online.

Tissue collection and histological analysis

Matched 2-mm punch biopsy specimens were obtained from each side of the face 2 months after the final treatment for the histological and immunohistochemical evaluation. The tissue samples were fixed in 10% buffered formalin and embedded in paraffin. Following deparaffinization and rehydration, standard protocols were employed to perform Masson's trichrome (MT) and hematoxylin and eosin (H&E) staining in 4-μm paraffin sections. Epidermal and full skin thicknesses were evaluated from H&E-stained sections, and collagen deposition in the papillary and reticular dermis was quantified from the MT-stained images. Detailed quantitative analysis methods are presented in the Supplementary Materials and Methods section online.

Immunohistochemical analysis

4-μm paraffin sections were deparaffinized, rehydrated in ethanol, and subjected to heat-mediated antigen retrieval in pH 9 Target Retrieval Solution (S2367; Dako, Carpinteria, CA, USA) or pH 6 Citrate Buffer (CBB999, ScyTek Laboratories, Logan, UT, USA) at 120 °C for 10 min using a pressure cooker. After permeabilization with 0.1% Triton X-100 for 10 min, a serum-free blocking solution was added for 10 min at room temperature. The samples were incubated overnight at 4 °C with the following primary antibodies: HSP47, 1:1000 (ab226052; Abcam, Cambridge, UK); CD45, 1:200 (13917, Cell Signaling Technology, Danvers, MA, USA); CD68,

1:200 (M0814, Dako); $p16^{INK4A}$, prediluted (805–4713, Ventana Medical Systems, Oro Valley, AZ, USA); procollagen-1, 1:50 (SP1.D8; DSHB, Iowa City, IA, United States); elastin, 1:1000 (ab77804; Abcam); and ki-67, 1:1000 (ab16667; Abcam). Subsequently, they were incubated with fluorescent-labeled secondary antibodies for 1 h at room temperature. After staining with DAPI (1 μg/ml), immunofluorescence images were acquired using a Confocal Microscope (Leica STED CW; Leica Microsystems, Wetzlar, Germany). Detailed protocols for image analysis are outlined in the Supplementary Materials and Methods section online.

Statistical analysis

Comparison of interval changes in clinical skin parameters between baseline, 3 months, and 5 months was performed using repeated-measures analysis of variance. If the normality hypothesis of the data was rejected by the Shapiro-Wilk test or if the sphericity hypothesis of the data was violated according to Mauchly's test, the generalised estimated equation analysis or Wilks' Lambda multivariate test was performed. Subsequent post hoc analysis was conducted using the paired *t*-test or Wilcoxon signed-rank test with Bonferroni correction for multiple comparisons. For split-face comparison of histological findings, a paired *t*-test or Wilcoxon's signed-rank test was employed, contingent upon normality validation using the Shapiro-Wilk test. The chi-squared ($\chi 2$) test was conducted to compare the frequencies of adverse skin reactions following MN and MNRF treatments. Statistical significance was set at a p-value of < 0.05. SPSS Statistics 26.0 (IBM Corp., Armonk, NY, USA) was used for all the statistical analyses.

Data availability

The datasets generated during and/or analysed during the current study are available from the corresponding author on reasonable request.

Received: 19 December 2024; Accepted: 14 May 2025
Published online: 26 May 2025

References

1. Fernández, V., Gómez, F., Sandoval-García, A. & Cabrera-Rios, K. Signs of skin aging: a review. *Int. J. Res. Med. Sci.* **12**, 2674–2679 (2024).
2. Chung, J. H., Hanft, V. N. & Kang, S. Aging and Photoaging. *J. Am. Acad. Dermatol.* **49**, 690–697 (2003).
3. Zhang, Y. et al. Uncovering key mechanisms and intervention therapies in aging skin. *Cytokine Growth Factor. Rev.* **79**, 66–80 (2024).
4. Marcos-Garcés, V. et al. Age-related dermal collagen changes during development, maturation and ageing – a morphometric and comparative study. *J. Anat.* **225**, 98–108 (2014).
5. Chin, T., Lee, X. E., Ng, P. Y., Lee, Y. & Dreesen, O. The role of cellular senescence in skin aging and age-related skin pathologies. *Front Physiol* **14**, (2023).
6. Konstantinou, E., Longange, E. & Kaya, G. Mechanisms of senescence and Anti-Senescence strategies in the skin. *Biology* **13**, 647 (2024).
7. Wlaschek, M., Maity, P., Makrantonaki, E. & Scharffetter-Kochanek, K. Connective tissue and fibroblast senescence in skin aging. *J. Invest. Dermatol.* **141**, 985–992 (2021).
8. Kim, H. et al. Attenuation of intrinsic ageing of the skin via elimination of senescent dermal fibroblasts with senolytic drugs. *J. Eur. Acad. Dermatol. Venereol.* **36**, 1125–1135 (2022).
9. Pils, V. et al. Promises and challenges of senolytics in skin regeneration, pathology and ageing. *Mech. Ageing Dev.* **200**, 111588 (2021).
10. Spandau, D. F., Lewis, D. A., Somani, A. K. & Travers, J. B. Fractionated laser resurfacing corrects the inappropriate UVB response in geriatric skin. *J. Invest. Dermatol.* **132**, 1591–1596 (2012).
11. Kim, M., Kim, S. M., Kwon, S., Park, T. J. & Kang, H. Y. Senescent fibroblasts in melasma pathophysiology. *Exp. Dermatol.* **28**, 719–722 (2019).
12. Kwon, S. H., Na, J. I., Huh, C. H. & Park, K. C. A clinical and biochemical evaluation of a Temperature-Controlled continuous Non-Invasive radiofrequency device for the treatment of melasma. *Ann. Dermatol.* **33**, 522–530 (2021).
13. Yoon, J. E. et al. Senescent fibroblasts drive ageing pigmentation: A potential therapeutic target for senile Lentigo. *Theranostics* **8**, 4620–4632 (2018).
14. Lee, Y. I. et al. Synergistic effect of 300 Mm Needle-Depth fractional microneedling radiofrequency on the treatment of Senescence-Induced aging hyperpigmentation of the skin. *Int. J. Mol. Sci.* **22**, 7480 (2021).
15. Hantash, B. M., Renton, B., Berkowitz, R. L., Stridde, B. C. & Newman, J. Pilot clinical study of a novel minimally invasive bipolar microneedle radiofrequency device. *Lasers Surg. Med.* **41**, 87–95 (2009).
16. Serdar, Z. A. & Tatlıparmak, A. Comparison of efficacy and safety of fractional radiofrequency and fractional Er:YAG laser in facial and neck wrinkles: Six-year experience with 333 patients. *Dermatol. Ther.* **32**, e13054 (2019).
17. Liu, T. M., Sun, Y., -M., Tang, Z. Y., Li, Y. & -H Microneedle fractional radiofrequency treatment of facial Photoageing as assessed in a split-face model. *Clin. Exp. Dermatol.* **44**, e96–e102 (2019).
18. Kwon, S. H. et al. The efficacy and safety of microneedle monopolar radiofrequency for the treatment of periorbital wrinkles. *J. Dermatol. Treat.* **32**, 460–464 (2021).
19. Lee, S. J. et al. Consensus recommendations on the use of a fractional radiofrequency microneedle and its applications in dermatologic laser surgery. *Med. Lasers.* **3**, 5–10 (2014).
20. Ibrahim, O., Munavalli, G. S. & Dover, J. S. Radiofrequency with microneedling. *Adv. Cosmet. Surg.* **1**, 109–115 (2018).
21. Bipolar fractional radiofrequency treatment induces neoelastogenesis. and neocollagenesis - Hantash – 2009 - Lasers in Surgery and Medicine - Wiley Online Library. https://onlinelibrary-wiley-com-ssl.libproxy.snu.ac.kr/doi/https://doi.org/10.1002/lsm.20731
22. Gershonowitz, A. & Gat, A. VoluDerm microneedle technology for skin treatments—In vivo histological evidence. *J. Cosmet. Laser Ther.* **17**, 9–14 (2015).
23. Kauvar, A. N. B. & Gershonowitz, A. Clinical and histologic evaluation of a fractional radiofrequency treatment of wrinkles and skin texture with novel 1-mm long ultra-thin electrode pins. *Lasers Surg. Med.* **54**, 54–61 (2022).
24. Zhang, J., Yu, H., Man, M. Q. & Hu, L. Aging in the dermis: fibroblast senescence and its significance. *Aging Cell.* **23**, e14054 (2024).
25. Ressler, S. et al. p16INK4A is a robust in vivo biomarker of cellular aging in human skin. *Aging Cell.* **5**, 379–389 (2006).
26. Ohtani, N. The roles and mechanisms of senescence-associated secretory phenotype (SASP): can it be controlled by senolysis? *Inflamm. Regen.* **42**, 11 (2022).

27. El-Domyati, M. et al. Multiple microneedling sessions for minimally invasive facial rejuvenation: an objective assessment. *Int. J. Dermatol.* **54**, 1361–1369 (2015).
28. Cohen, B. E. & Elbuluk, N. Microneedling in skin of color: A review of uses and efficacy. *J. Am. Acad. Dermatol.* **74**, 348–355 (2016).
29. Alexiades-Armenakas, M. et al. Randomized, quantitative grading comparison of minimally invasive, fractional radiofrequency and surgical Face-lift to treat skin laxity. *Arch. Dermatol.* **146**, 396–405 (2010).
30. Tanaka, Y. Long-term three-dimensional volumetric assessment of skin tightening using a sharply tapered non-insulated microneedle radiofrequency applicator with novel fractionated pulse mode in Asians. *Lasers Surg. Med.* **47**, 626–633 (2015).

Author contributions

Jung Min Hwang: Conceptualization, Visualization, Formal analysis, Investigation, Resources, Writing – original draft preparation, Writing - review & editing. Soo Hyun Lee: Conceptualization, Visualization, Formal analysis, Investigation. Eun Jae Baek: Conceptualization, Visualization, Investigation. Hye-Rin Charlotte Kim: Conceptualization, Visualization, Investigation. Jang-Hee Oh: Conceptualization, Formal analysis, Resources. Ji Su Lee: Conceptualization, Resources. Si-Hyung Lee: Conceptualization, Funding acquisition, Project administration, Resources, Supervision, Writing – review & editing.

Declarations

Competing interests

. Si-Hyung Lee received research funding and device support from Viol Co., Ltd. for this study. The company had no role in study design, data collection, analysis, or manuscript preparation. The authors declare no other competing interests.

Additional information

Supplementary Information The online version contains supplementary material available at https://doi.org/10.1038/s41598-025-02545-3.

Correspondence and requests for materials should be addressed to S.-H.L.